Materials Science and Engineering A 527 (2010) 7865–7872

Contents lists available at ScienceDirect

Materials Science and Engineering A

journal homepage: www.elsevier.com/locate/msea

Constitutive flow behavior and hot workability of powder metallurgy processed 20 vol.%SiC_P/2024Al composite

J.C. Shao, B.L. Xiao, Q.Z. Wang, Z.Y. Ma*, Y. Liu, K. Yang

Shenyang National Laboratory for Materials Science, Institute of Metal Research, Chinese Academy of Sciences, 72 Wenhua Road, Shenyang 110016, China

ARTICLE INFO

Article history:
Received 4 July 2010
Received in revised form 20 August 2010
Accepted 26 August 2010

Keywords:
Metal matrix composites
Constitutive equations
Processing maps
Aluminum alloys
Powder metallurgy

ABSTRACT

Constitutive flow behavior and hot workability of the powder metallurgy processed 20 vol.%SiC_P/2024Al composite were investigated using hot compression tests. The modified Arrhenius-type constitutive equations were presented with the values of material constants in consideration as a function of strain. Dynamic material model (DMM) and modified DMM were used to construct the power dissipation efficiency maps, and Ziegler's instability criterion and Gegel's stability criterion were used to build instability maps. The presence of finer SiC_P and more boundaries resulting from smaller 2024Al powders shifted the dynamic recrystallization domain of the 2024Al matrix to higher strain rate and lower temperature ranges and decreased the peak value of power dissipation efficiency. Large instable regions were found in the form of flow localization and cavitations located at the matrix/SiC_P interfaces and within the SiC_P clusters. By comparison, the Gegel's stability criterion was more sensitive to the instability zones than the Ziegler's instability criterion for this material.

1. Introduction

Aluminum matrix composites (AMCs) reinforced with SiC_P are recognized as important advanced structural materials due to their desirable properties, including high specific stiffness, high specific strength, high-temperature resistance and improved wear resistance [1–3]. However, the workability of the AMCs is greatly restricted by the incompatible deformation of the soft matrix and the hard reinforcements [4–7]. Moreover, the stress concentration at the matrix–particle interfaces produces high levels of damages, which include particle fracture and decohesion [2,4,8]. For these reasons, the workability of the SiC_P reinforced AMCs is very sensitive to processing parameters such as temperature and strain rate, and the processing parameters have to be optimized for each composite system.

The flow behavior of materials during hot working process is relevant to the flow stress (σ), which can be represented mathematically as a function of strain (ε), strain rate ($\dot{\varepsilon}$) and temperature (T). Hence, a thorough understanding of the constitutive flow equations of a material under processing conditions is essential for the optimization of processing parameters. Arrhenius-type constitutive equations have been usually applied to the particle reinforced AMCs [5,9–13], but less attention was paid to the effect of strain on the constitutive flow softening behavior of these materials.

Though the constitutive flow equations are considered to contain some information related to the deformation mechanisms, it is implicit, and similar stress–strain curves may stand for different deformation mechanisms. Therefore, it is not advisable to conclude on the deformation mechanisms just from the stress–strain curves, especially for materials with complex microstructures. Implementing the flow stress data into the dynamic material model (DMM), the processing maps developed by Prasad et al. [14,15] and modified by Narayana Murty et al. [16,17] have been used to study the hot workability of metal matrix composites [15,18–32]. Workability of the SiC_P reinforced AMCs depends upon the initial microstructures which are determined by the preparation method, prior processing history, grain size, volume fraction and size of SiC_P. Though some investigators have studied the hot workability of the SiC_P reinforced AMCs during the past two decades [15,18,19,21,26,27,30], the sizes of the SiC_P were 10–30 μm and the sizes of Al alloy matrix powders were 30–50 μm in their composite systems. Few investigations have been carried out to study the hot workability of the AMCs fabricated with finer SiC_P and smaller Al alloy powders.

In this work, the constitutive flow equations of a powder metallurgy (PM) processed 20 vol.%SiC_P/2024Al composite (SiC_P with a nominal size of 3.5 μm and 2024Al powders with an average diameter of 13 μm) was examined. Power dissipation efficiency maps based on the DMM and modified DMM and instability zones based on Ziegler's instability criterion and Gegel's stability criterion were generated to evaluate the hot workability, elucidate the hot deformation mechanisms and optimize the processing parameters of this material.

* Corresponding author. Tel.: +86 24 83978908; fax: +86 24 83978908.
E-mail address: zyma@imr.ac.cn (Z.Y. Ma).

0921-5093/$ – see front matter © 2010 Elsevier B.V. All rights reserved.
doi:10.1016/j.msea.2010.08.080

2. Experimental

The 20 vol.%SiC_P/2024Al composite was produced through the PM route. The 2024Al powders (Al–4.5 wt.%Cu–1.5 wt.%Mg), with an average diameter of 13 μm, were blended with a volume fraction of 20% α-SiC particles (with a nominal size of 3.5 μm) for 8 h, and subsequently cold compacted. Then the as-compacted green billet was consolidated by hot-pressing at 585 °C and at a pressure of 80 MPa for 1 h in vacuum.

Cylindrical compressive specimens 8 mm in diameter and 12 mm in height were machined from those hot-pressing-sintered billets. Uniaxial compression tests were conducted in the temperature range of 400–475 °C (in step of 25 °C) and the strain rate range of 0.001–1.0 s^{-1}, utilizing Gleeble 3800 to achieve isothermal constant strain rate deformation. Specimens were coated with MoS_2 lubricant to ensure homogeneous deformation. The specimens were heated at 5 K/s up to the deformation temperature, held for 10 min and then compressed. In experimental process, the micro-processor of Gleeble collected the data automatically and obtained true stress–strain curves using standard equations. Deformed specimens were water quenched and sectioned parallel to the compression axis, and then mechanically polished and etched with Keller's reagent. The specimens were examined by optical and scanning electron microscopy (OM and SEM).

3. Results

3.1. Initial microstructure

Fig. 1(a) shows the optical micrograph of the hot-pressing-sintered composite, which was slightly etched. The microstructure of the composite was characterized by clear prior particle boundaries (PPBs, denoted with black arrows in Fig. 1(a)) of the Al particles and a chain-like distribution of the SiC_P around the Al particles. There are some copper red phases within the SiC_P clusters and the back-scattered electron (BSE) image shows that they are white (Fig. 1(b)). The EDS analysis confirms that the main elements are aluminum and copper (Fig. 1(c)), indicating the generation of Al–Cu phases.

3.2. Determination of constitutive equations

The characteristic compressive stress–strain curves of the composite are shown in Fig. 2. It could be observed that the influence of the temperature and strain rate on the flow stress is significant. The flow curve exhibits an initial strain hardening, and after a peak stress it is followed by a steady state at low strain rates and by a softening at higher strain rates. During the hot deformation process, dynamic recovery (DRV), dynamic recrystallization (DRX) and strain hardening occur simultaneously. For the flow stress curve which undergoes DRX, generally, as the strain increases the flow stress increases up to a peak stress which is caused by the balance between the softening due to DRX and the strain hardening in the uncrystallized parts of the material, and then decreases until it reaches a steady state.

The constitutive flow behavior of this material can be described by a phenomenological power–Arrhenius relationship, as follows:

$$\dot{\varepsilon} = A\sigma^n \exp\left(\frac{-Q}{RT}\right) \quad (1)$$

where A and n are material constants, $\dot{\varepsilon}$ is the strain rate (s^{-1}), σ is the flow stress (MPa), Q is the apparent activation energy of deformation (kJ/mol), R is the gas constant (kJ/mol K^{-1}) and T is the absolute temperature (K). The average values of n can be calculated from the slope of the linearly fitted lines in the $\ln\sigma - \ln\dot{\varepsilon}$ plot in Fig. 3(a). From Fig. 3(b), the average Q value at a strain of 0.5 is calculated to be 279 kJ/mol, which is significantly higher than the activation energy for self-diffusion in pure aluminum (142 kJ/mol). The higher Q value in the composite is due to the effect of SiC_P which pins the motion of the dislocations and grain boundaries and raises the deformation resistance.

Then, the three material constants, n, A and Q, determined at strains ranging from 0.1 to 0.7 with an interval of 0.05, are plotted and fitted using fourth-order polynomial equations in Fig. 4. The fitted curves are close to the experimental data as all the R-squares between fitted and experimental data are above 0.972. The fitted equations for the three material constants are the functions of strain as shown in Eqs. (2)–(4):

$$n = 14.035\varepsilon^4 - 27.467\varepsilon^3 + 17.455\varepsilon^2 - 2.961\varepsilon + 7.614 \quad (2)$$

$$A = (-19.988\varepsilon^4 - 39.854\varepsilon^3 + 58.539\varepsilon^2 - 18.158\varepsilon + 4.197) \times 10^5 \quad (3)$$

$$Q = 149\varepsilon^4 - 454.8\varepsilon^3 + 357.3\varepsilon^2 - 80.9\varepsilon + 277.56 \quad (4)$$

Eqs. (1)–(4) are used to construct the constitutive equations of the 20 vol.%SiC_P/2024Al composite at the strain rates from 0.001 to 1.0 s^{-1} and the temperatures from 400 to 475 °C. Fig. 5 shows the comparisons between the experimental flow curves and the ones predicted by the developed constitutive equations under different strain rates for four testing temperatures, while considering the compensation of strain. It is noted that the predicted flow stress values could track the experimental data throughout the entire strain range for various testing conditions. Though Eqs. (1)–(4) give a good description of the flow stress for the present SiC_P/2024Al composite, the discrepancies between the experimental data and the predicted results using Eqs. (1)–(4) exist, as shown in Fig. 5. The main reason is that the flow stress versus strain rate does not obey power-law at any strain and temperature for the present SiC_P/2024Al composite, and Eqs. (1)–(4) just give an approximate prediction.

3.3. Characterization of processing maps

3.3.1. DMM and modified DMM based power dissipation efficiency maps

In the DMM, material is considered to be a dissipater of power when it undergoes plastic flow to take the shape imposed by the die. This means that no storing of energy takes place (no strain hardening but steady state and softening occur) during deformation process. According to the DMM, at any strain and temperature, the power of dissipation P (per unit volume) can be separated into two phenomena: content G, power dissipated by plastic work, most of which is converted into heat; co-content J, power dissipated by dynamic metallurgical processes such as DRV, DRX, superplastic deformation, internal fracture (void formation or wedge cracking), etc. At a constant temperature and strain, the power P absorbed by the material at any given strain rate $\dot{\varepsilon}$ during deformation can be written as follows:

$$P_{\varepsilon,T} = \sigma\dot{\varepsilon} = G + J = \int_0^{\dot{\varepsilon}} \sigma d\dot{\varepsilon} + \int_0^{\sigma} \dot{\varepsilon} d\sigma \quad (5)$$

From Eq. (5), it follows that at any given strain and temperature, the change in J with respect to G yields the strain rate sensitivity parameter m, which is,

$$\left(\frac{\partial J}{\partial G}\right)_{\varepsilon,T} = \left(\frac{\sigma d\dot{\varepsilon}}{\dot{\varepsilon} d\sigma}\right)_{\varepsilon,T} = \left[\frac{\partial(\ln\sigma)}{\partial(\ln\dot{\varepsilon})}\right]_{\varepsilon,T} \simeq \left[\frac{\partial(\log\sigma)}{\partial(\log\dot{\varepsilon})}\right]_{\varepsilon,T} = m \quad (6)$$

Prasad et al. [14,15] assumed that the dynamic response of a material to the hot deformation could be represented by the power-law $\sigma = K\dot{\varepsilon}^m$ where the m was independent of $\dot{\varepsilon}$. The metallurgical

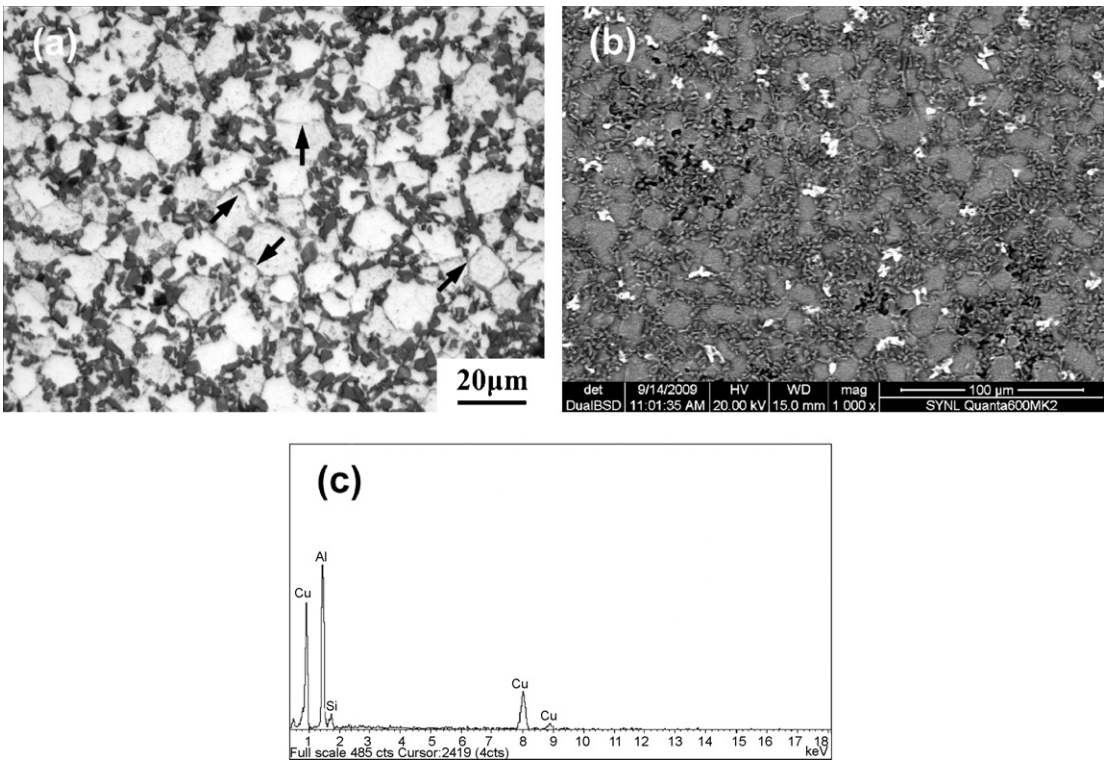

Fig. 1. Initial microstructures of hot-pressing-sintered 20 vol.%SiC_P/2024Al composite: (a) optical micrograph (black arrows indicate the prior particle boundaries), (b) SEM backs-scattered electron image and (c) energy dispersion analysis.

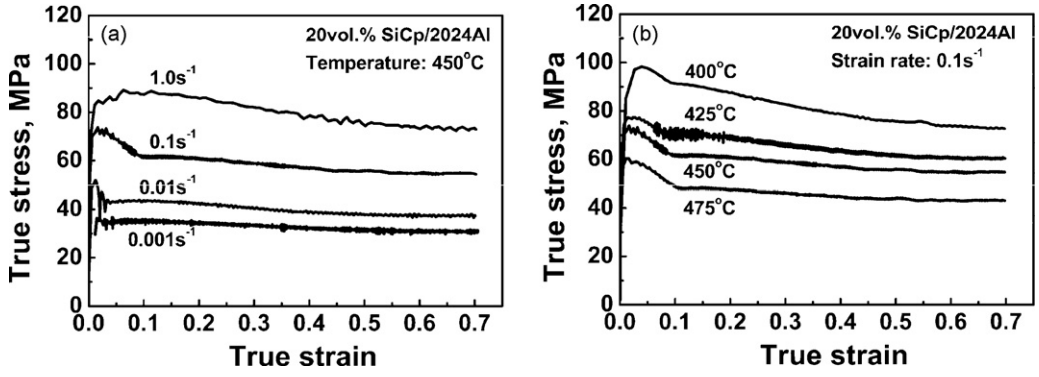

Fig. 2. Flow stress curves of 20 vol.%SiC_P/2024Al composite at (a) 450 °C for different strain rates and (b) 0.1 s^{-1} for different temperatures.

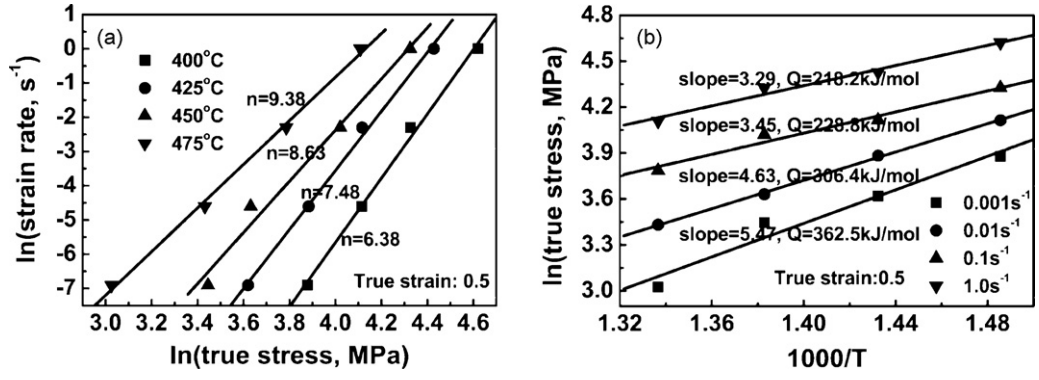

Fig. 3. Evaluating the value of (a) parameter n by plotting ln(true stress) versus ln(strain rate) and (b) activation energy Q by plotting ln(true stress) versus 1000/T.

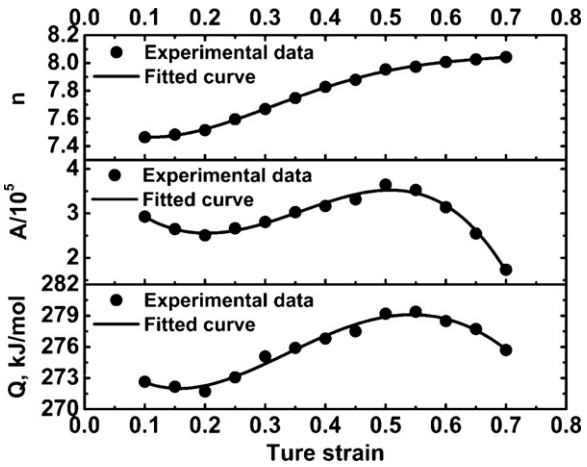

Fig. 4. Variation of n, A and activation energy Q with true strain (the data were fitted by the fourth-order polynomial equations).

dissipation process may be characterized by the variation of J co-content with strain, temperature and strain rate, but normalization with the input power (P) sharpens the variation. For an ideal plastic flow, the flow stress is proportional to the strain rate at any strain and temperature ($m = 1$). In this case, the value of J becomes $J_{max} = P/2$ which stands for a linear ideal dissipater in which maximum possible dissipation through J co-content occurs. Then, the power dissipation efficiency η was defined as [14,15]:

$$\eta = \frac{J}{J_{max}} = \frac{J}{P/2} = \frac{2m}{m+1} \tag{7}$$

The η is a dimensionless parameter which represents the relative rate of internal entropy production during hot deformation and characterizes how efficiently the material dissipates energy by microstructural changes. This parameter can be plotted as a function of temperature and strain rate to obtain the power dissipation efficiency map. This map exhibits several efficiency “hills” which appear as “domains” and represent a microstructural mechanism and “valleys” which are referred to as the bifurcation of neighboring domains.

Based on Ziegler's instability criterion [15,33] the instability parameter ξ_1 is defined as:

$$\xi_1 = \frac{\partial \ln(m/m+1)}{\partial \ln \dot{\varepsilon}} + m \le 0 \tag{8}$$

Considering that the flow stress does not strictly obey the power-law and m varies with $\dot{\varepsilon}$ and T in many alloys and composites, Narayana Murty and Nageswara Rao [16] proposed modifications to the DMM in which the power dissipation efficiency η could be calculated using the definition in Eq. (7), where J is derived from Eq. (5) as follows:

$$\eta = \frac{J}{J_{max}} = \frac{J}{P/2} = \frac{2(P-G)}{P} = 2\left(1 - \frac{G}{P}\right)_{\varepsilon,T},$$
$$G = \int_0^{\dot{\varepsilon}} \sigma d\dot{\varepsilon} = \int_0^{\dot{\varepsilon}_{min}} \sigma d\dot{\varepsilon} + \int_{\dot{\varepsilon}_{min}}^{\dot{\varepsilon}} \sigma d\dot{\varepsilon} = \left[\frac{\sigma\dot{\varepsilon}}{m+1}\right]_{\dot{\varepsilon}=\dot{\varepsilon}_{min}} + \int_{\dot{\varepsilon}_{min}}^{\dot{\varepsilon}} \sigma d\dot{\varepsilon} \tag{9}$$

where $\dot{\varepsilon}_{min}$ is the minimal experimental strain rate (0.001 s^{-1} here) and the value of m at $\dot{\varepsilon}_{min}$ can be calculated from the derivative of $\log\sigma - \log\dot{\varepsilon}$ curve fitted with a cubic spline or a third-order polynomial. The second integral can be obtained from the area below the experimental value of σ connected linearly with the $\dot{\varepsilon}$ axis using trapezoidal rule.

The instability parameter ξ_2 based on the Ziegler's criterion considered by Narayana Murty et al. [16,17] can be written as:

$$\xi_2 = \frac{2m}{\eta} - 1 < 0 \tag{10}$$

which is valid when $m > 0$.

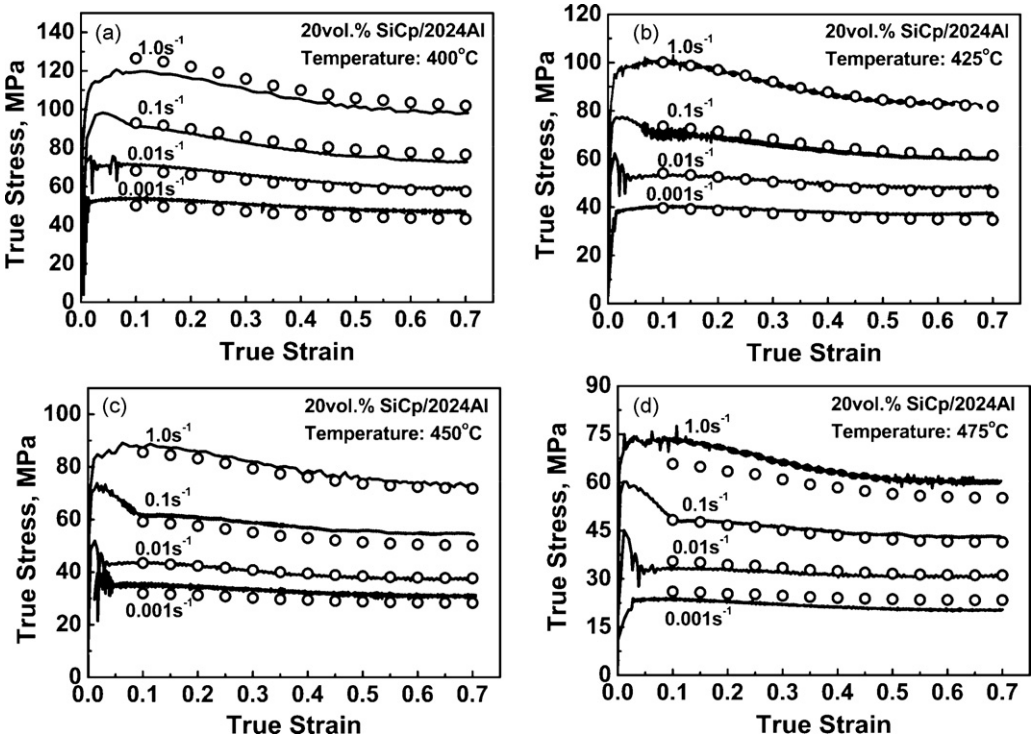

Fig. 5. Comparisons between predicted and measured flow stress curves (the open circles denote the predicted results and the lines denote the experimental data) at (a) 400 °C, (b) 425 °C, (c) 450 °C and (d) 475 °C.

In contrast, Gegel et al. [34] used the Lyaponov function and suggested a different stability criterion. The instability parameters ξ_3–ξ_6 based on Gegel's stability criterion are:

$$\xi_3 = m < 0 \tag{11}$$

$$\xi_4 = -\frac{\partial \eta}{\partial(\ln \dot{\varepsilon})} < 0 \tag{12}$$

$$\xi_5 = s - 1 < 0 \tag{13}$$

$$\xi_6 = -\frac{\partial s}{\partial(\ln \dot{\varepsilon})} < 0 \tag{14}$$

where s is the temperature sensitivity of flow stress and can be written as $s = (1/T)(\partial(\ln\sigma)/\partial(1/T))|_{\varepsilon,\dot{\varepsilon}}$.

3.3.2. Processing maps at a strain of 0.4

Both the DMM and the modified DMM were applied to analyze the data in the present study. In order to identify the microstructural instability, different instability criteria presented in the preceding section were examined and compared. A strain of 0.4 was selected since it was sufficiently large for softening processes, such as DRV and DRX, to come into play but not so large for non-uniform deformation to occur.

The power dissipation efficiency maps of the 20 vol.%SiC_P/2024Al composite at a strain of 0.4 are shown in Fig. 6(a) and (b). Both of these two power dissipation efficiency maps which were produced by the DMM and the modified DMM, respectively, exhibit two domains:

(1) Domain A, occurring at 400–430 °C and 0.001–0.006 s^{-1} for the DMM based processing map (Fig. 6(a)), and at 400–430 °C and 0.001–0.003 s^{-1} for the modified DMM based processing map (Fig. 6(b)), has a peak efficiency of about 25%.
(2) Domain B, occurring at 440–475 °C and 0.01–0.3 s^{-1} for the DMM based processing map (Fig. 6(a)), and at 440–475 °C and of 0.03–1.0 s^{-1} for the modified DMM based processing map (Fig. 6(b)), has a peak efficiency of about 30%.

Though the general configurations of these two maps are similar, the figures differ in several details. It is apparent that domain A moves to the lower strain rate range and domain B moves to the higher strain rate range in the modified DMM based processing map compared with the DMM based processing map. These discrepancies are mainly due to the assumption of power-law flow stress distribution when computing η in Eq. (7) which is valid for the flow stress at any strain and temperature obeying the power-law [16]. If the flow stress does not strictly obey the power-law, Eq. (7) becomes inaccurate or even erroneous. Eq. (9) proposed in the modified DMM is valid whether the flow stress versus strain rate obeys the power-law or not. Consequently, the modified DMM based processing map is more accurate for the present SiC_P/2024Al composite.

Figs. 7 and 8 show the instability zones (shaded zones) for the DMM and the modified DMM which were predicted by the Ziegler's instability criterion according to Eqs. (8) and (10) and by the Gegel's stability criterion according to Eqs. (11)–(14), respectively. For complicated alloys and composites, the flow stress with respect to $\dot{\varepsilon}$ does not obey power-law and the assumption and computation of Eq. (8) is conflict and erroneous. By comparison, Eq. (10) which is derived based on the Ziegler's criterion is valid whether the flow stress versus strain rate obeys the power-law or not. Apart from the instability criterion based on the Ziegler's criterion, the Gegel's stability criterion based on Lyaponov criteria is considered also. It can be seen from the comparison of Figs. 7 and 8 that the Gegel's stability criterion yields larger and even conflicting results about the identification of regions of instability compared to the Ziegler's instability criterion. In fact, there is no unique instability theory which leads the designer to establish the most suitable instability maps for complicated materials. In the case of damage, the local state of stress plays a significant role and the detailed microstructural investigations are required to identify the metallurgical processes and the unstable flow regions.

4. Discussion

4.1. Interpretation of power dissipation efficiency maps

During the hot deformation process of the SiC_P reinforced AMCs, the flow behavior of the composite is mainly governed by the microstructural transformations and the matrix flow constrained by the hard particles. These two processes dissipate the provided power and can be reflected in the power dissipation efficiency map.

Domain A is characterized by steady state flow curves (Fig. 5) and a peak efficiency of about 25% (Fig. 6). Compared to the hot-pressing-sintered composite with the PPBs (Fig. 1(a)), typical macrostructure obtained at 400 °C and 0.001 s^{-1} within this domain reveals elongated grains (Fig. 9(a)) which represents typical feature of DRV. In previous studies [15,18–27,29–31], only a few investigators [15,18,31] reported that DRV was found in particles or whiskers reinforced AMCs at low temperatures (300–350 °C) and low strain rates (0.001–0.01 s^{-1}). The DRV process is controlled by the slipping and climbing of dislocations. There were lots of boundaries in the hot-pressing-sintered composite fabricated using smaller 2024Al powders. These boundaries combined with SiC_P, oxide particles and precipitates pin the dislocation movement and reduce the rate of DRV, thereby shifting the deformation conditions for DRV to higher temperatures and lower strain rates.

Domain B is characterized by softened flow curves (Fig. 5) and a peak efficiency of about 30% (Fig. 6). Typical macrostructure obtained at 450 °C and 0.1 s^{-1} within this domain is shown in Fig. 9(b). The deformed microstructure exhibits considerable reconstitution of the PPBs and a fine-grained structure as a result of DRX. DRX is a beneficial process during hot deformation process since it not only gives stable flow but also reconstitutes the microstructure of the PM compacts. Though in most of Al alloys DRX does not occur normally, DRX has been confirmed in particles or whiskers reinforced AMCs [18–27,30,31].

DRX is considered to be a process in terms of the rate of interface formation (nucleation) and the rate of interface migration (growth) [35]. The interface formation rate depends on the rate of dislocation generation, resulting in the formation of subgrain structure, and the interface migration rate depends upon the diffusion coefficient and driving force. The composite in this study was fabricated with finer SiC_P and smaller 2024Al powders compared to the previous reports. The finer SiC_P induces the higher rate of dislocation generation in the vicinity of finer SiC_P during hot deformation process. Then the interface formation is further enhanced due to the high rate of dislocations generation near the finer SiC_P which is a preferred site for the development of a recrystallization nucleus [18,21,27]. At the same time, the higher density of dislocation causes the formation of very fine subgrain structure, which enhances the rate of interface migration and reduces the DRX temperature. Radhakrishna Bhat et al. [18] compared the DRX domain of extruded SiC_P/Al composite with that of sintered composite and attributed the increase in the strain rate for DRX to smaller grain size in the extruded composite. Therefore, the DRX domain of the composite shifts to higher strain rates and lower temperatures range. Generally, the peak value of η for DRX ranges from 35 to 50% in the Al alloys, but this value decreases in the AMCs. The reason is that the power dissipated by plastic work increases during hot deformation because large volume of finer SiC_P and lots of 2024Al particle boundaries in

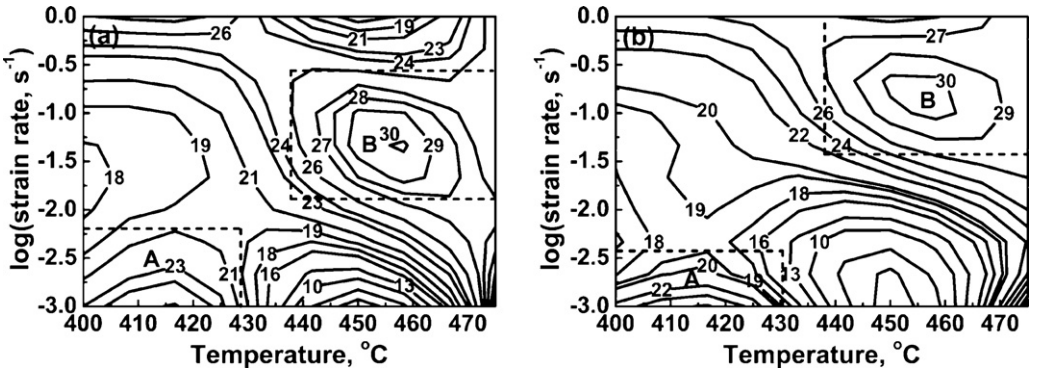

Fig. 6. Power dissipation efficiency maps of 20 vol.%SiC_P/2024Al composite at a strain of 0.4 constructed by (a) DMM and (b) modified DMM.

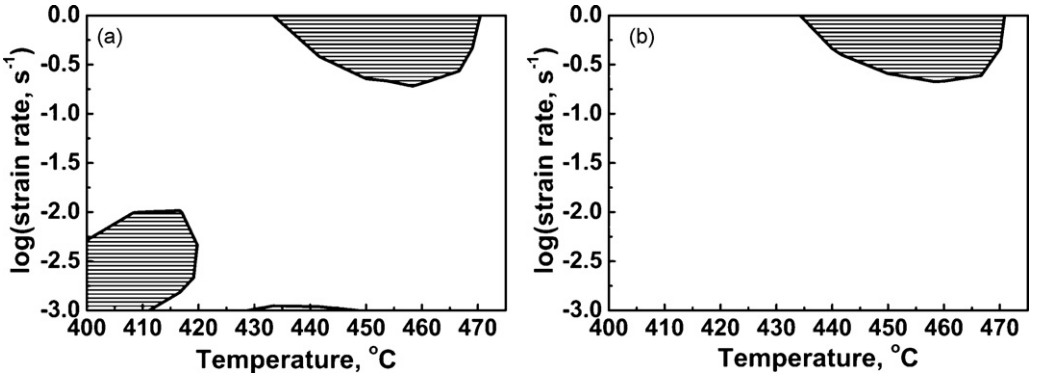

Fig. 7. Instability zones (shaded zones) of 20 vol.%SiC_P/2024Al composite at a strain of 0.4 based on Ziegler's instability criteria: (a) DMM and (b) modified DMM.

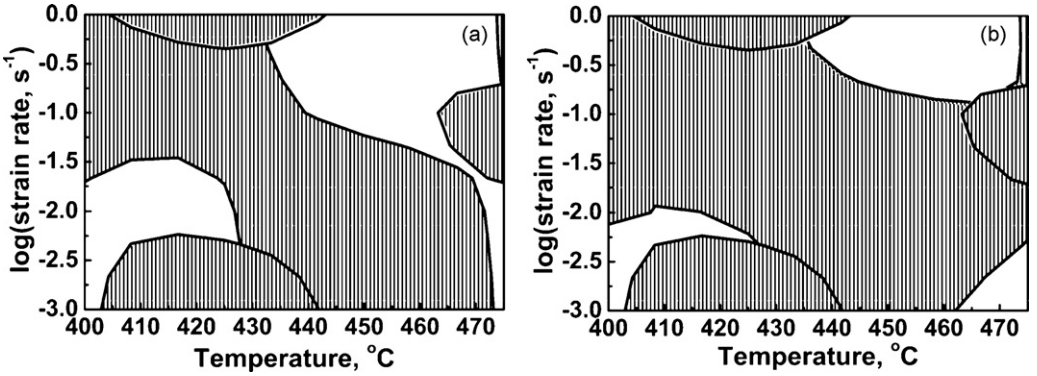

Fig. 8. Instability zones (shaded zones) of 20 vol.%SiC_P/2024Al composite at a strain of 0.4 based on Gegel's stability criteria: (a) DMM and (b) modified DMM.

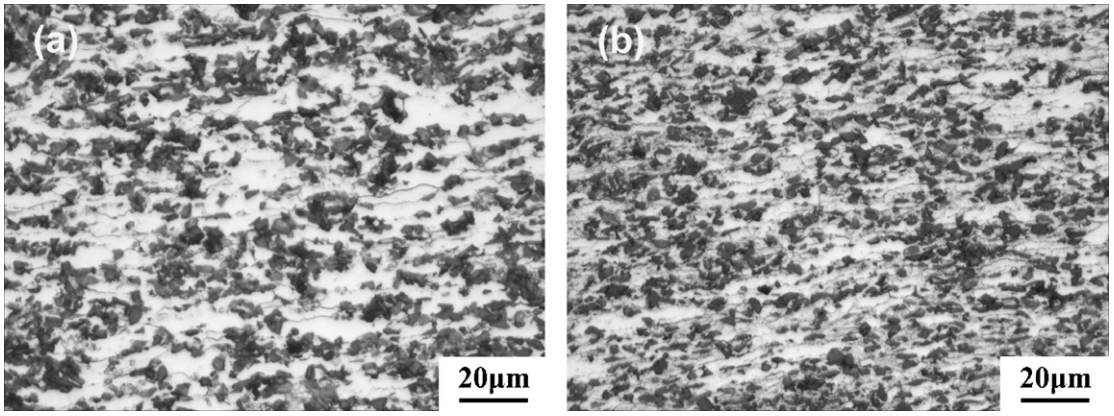

Fig. 9. Optical micrographs of 20 vol.%SiC_P/2024Al composite specimens tested at (a) 400 °C and 0.001 s^{-1} and (b) 450 °C and 0.1 s^{-1}.

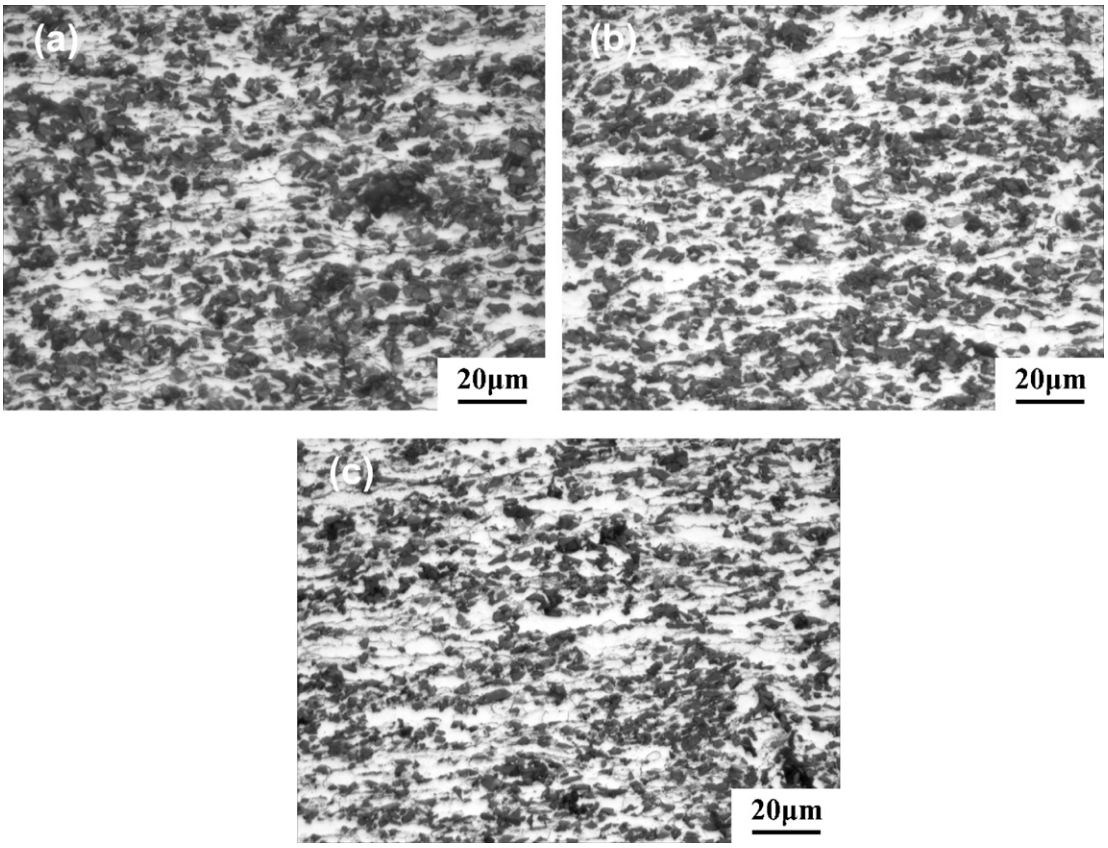

Fig. 10. Optical micrographs of 20 vol.%SiC_P/2024Al composite specimens tested at (a) 400 °C and 1.0 s^{-1}, (b) 425 °C and 0.001 s^{-1} and (c) 450 °C and 0.01 s^{-1}.

the composite raise the flow stress of the AMCs. Then the η value decreases according to Eqs. (5) and (9).

In addition to DRV and DRX, superplasticity was also observed in the particles or whiskers reinforced AMCs at higher temperatures and lower strain rates than those for DRX [18–21,26,27]. The basic mechanisms of superplasticity are the grain boundary sliding and diffusion which accommodates flow at grain boundary triple junctions and mitigate the formation of wedge cracks. However, Raj and Ramanathan et al. [30,36] proposed that if the strain rate was slow and the interfaces were weak, there would be enough time to relax the high stress concentration at the triple junctions and wedge cracking would occur. From Figs. 6(a) and (b) we can see that superplasticity phenomenon does not appear in the power dissipation efficiency maps, though this material has a fine-grained structure. The reason is that the hot-pressing-sintered composite has weak links between 2024Al particles because of the PPBs, and these provide ready paths for crack propagation.

4.2. Manifestation of instability

Optical micrographs of the 20 vol.%SiC_P/2024Al composite deformed at various conditions are shown in Fig. 10(a)–(c). The instability is observed in the form of flow localization and damage such as cavitations, which locate at the matrix/SiC_P interfaces and within the SiC_P clusters. When loading, the significant difference in elastic moduli between matrix and SiC_P induces stress concentration. This leads to rigid body movement of SiC_P and inhomogeneous deformation flow of the soft matrix, inducing flow localization and SiC_P clustering. If the tensile stress generated near the matrix/SiC_P interface does not have enough time to accommodate and exceeds the strength of interface, cavities would occur. Under the tensile state of stress, these cavities grow, coalesce, and cause damage. Though the damage at the matrix/SiC_P interface is driven by the local state of stress and cannot be represented as a characteristic domain in the power dissipation efficiency map, which reflects only the intrinsic response of the matrix material [23,28], it affects the measured flow stress and the instability map to a certain extent. As shown in Figs. 7 and 8, the composite exhibits larger instable regions according to the Gegel's stability criterion compared with the Ziegler's instability criterion. The microstructure of the material in all investigated conditions leads to the conclusion that the Gegel's stability criterion is more sensitive to the instability zones than the Ziegler's instability criterion for this composite. Then strictly processing parameters should be assigned according to Gegel's stability criterion. This will be very useful to determine hot working processing parameters and avoid instability and damage for this composite.

5. Conclusions

(1) Constitutive equations coupling flow stress with strain, strain rate and temperature were presented using the modified Arrhenius-type constitutive equations. A fourth-order polynomial was found to be adequate to represent the influence of strain on material constants with very good correlation.
(2) Both the DMM and the modified DMM were applied to analyze the power dissipation efficiency maps at a strain of 0.4. DRV and DRX were revealed in the power dissipation efficiency maps and verified by the microstructure examinations. Though the general configurations of processing maps based on these two models were similar, the figures differed in several details such as the location of metallurgical characteristic domains. The modified DMM based processing map is more accurate for the present SiC_P/2024Al composite.

(3) DRX was characterized by reconstitution of the PPBs and fine-grained structure. The finer SiC_P and lots of boundaries resulting from smaller 2024Al powders in the composite contributed to shifting the DRX domain to higher strain rates and lower temperatures and decreased the peak value of power dissipation efficiency.
(4) The PPBs weakened links between 2024Al particles and provided ready paths for crack propagation during hot deformation process. Therefore the superplasticity did not appear in this material.
(5) The composite exhibited large regions of instability in the form of flow localization and cavitations which located at the matrix/SiC_P interfaces and within the SiC_P clusters. The Gegel's stability criterion was more sensitive to the instability zones than the Ziegler's instability criterion for this material.

References

[1] T.W. Clyne, P.J. Withers, An Introduction to Metal Matrix Composites, Cambridge University Press, 1993.
[2] D.J. Lloyd, Int. Mater. Rev. 39 (1994) 1–23.
[3] J.M. Torralba, C.E. Da Costa, F. Velasco, J. Mater. Process. Technol. 133 (2003) 203–206.
[4] L.M. Tham, M. Gupta, L. Cheng, Mater. Sci. Eng. A 326 (2002) 355–363.
[5] P. Cavaliere, Composites A 35 (2004) 619–629.
[6] V.C. Srivastava, V. Jindal, V. Uhlenwinkel, K. Bauckhage, Mater. Sci. Eng. A 477 (2008) 86–95.
[7] L. Ceschini, G. Minak, A. Morri, Compos. Sci. Technol. 69 (2009) 1783–1789.
[8] C. Li, F. Ellyin, Mater. Sci. Eng. A 214 (1996) 115–121.
[9] X.X. Xia, H.J. McQueen, P. Sakaris, Scr. Mater. 32 (1995) 1185–1190.
[10] X.X. Xia, H.J. McQueen, Appl. Compos. Mater. 4 (1997) 333–347.
[11] S. Spigarelli, E. Evangelista, E. Cerri, T.G. Langdon, Mater. Sci. Eng. A 319 (2001) 721–725.
[12] E. Evangelista, S. Spigarelli, Metall. Mater. Trans. A 33 (2002) 373–381.
[13] E.M. Herba, H.J. McQueen, Mater. Sci. Eng. A 372 (2004) 1–14.
[14] Y.V.R.K. Prasad, H.L. Gegel, S.M. Doraivelu, J.C. Malas, J.T. Morgan, K.A. Lark, D.R. Barker, Metall. Trans. A 15 (1984) 1883–1892.
[15] Y.V.R.K. Prasad, S. Sasidhara, Hot Working Guide: A Compendium of Processing Maps, ASM International, Materials Park, Ohio, 1997.
[16] S.V.S. Narayana Murty, B. Nageswara Rao, Mater. Sci. Eng. A 254 (1998) 76–82.
[17] S.V.S. Narayana Murty, B. Nageswara Rao, B.P. Kashyap, Int. Mater. Rev. 45 (2000) 15–26.
[18] B.V. Radhakrishna Bhat, Y.R. Mahajan, H.M.D. Roshan, Y.V.R.K. Prasad, J. Mater. Sci. 27 (1992) 2141–2147.
[19] B.V. Radhakrishna Bhat, Y.R. Mahajan, H.M.D. Roshan, Y.V.R.K. Prasad, Mater. Trans. A 23 (1992) 2223–2230.
[20] B.V. Radhakrishna Bhat, Y.R. Mahajan, Mater. Sci. Eng. A 189 (1994) 137–145.
[21] B.V. Radhakrishna Bhat, Y.R. Mahajan, Y.V.R.K. Prasad, Metall. Mater. Trans. A 31 (2000) 629–639.
[22] E. Cerri, S. Spigarelli, E. Evangelista, P. Cavaliere, Mater. Sci. Eng. A 324 (2002) 157–161.
[23] S. Spigarelli, E. Cerri, P. Cavaliere, E. Evangelista, Mater. Sci. Eng. A 327 (2002) 144–154.
[24] S.V.S. Narayana Murty, B. Nageswara Rao, B.P. Kashyap, Compos. Sci. Technol. 63 (2003) 119–135.
[25] P. Cavaliere, E. Cerri, P. Leo, Compos. Sci. Technol. 64 (2004) 1287–1291.
[26] G. Ganesan, K. Raghukandan, R. Karthikeyan, B.C. Pai, Mater. Sci. Eng. A 369 (2004) 230–235.
[27] B.L. Xiao, J.Z. Fan, X.F. Tian, W.Y. Zhang, L.K. Shi, J. Mater. Sci. 40 (2005) 5757–5762.
[28] R.B. Bhat, S. Tamirisakandala, D.B. Miracle, V.A. Ravi, Metall. Mater. Trans. A 36 (2005) 845–857.
[29] S.V.S. Narayana Murty, B. Nageswara, B.P. Kashyap, J. Mater. Process. Technol. 166 (2005) 279–285.
[30] S. Ramanathan, R. Karthikeyan, G. Ganasen, Mater. Sci. Eng. A 441 (2006) 321–325.
[31] M. Vedani, F. D'Errico, E. Gariboldi, Compos. Sci. Technol. 66 (2006) 343–349.
[32] C. Poletti, H.P. Degischer, S. Kremmer, W. Marketz, Mater. Sci. Eng. A 486 (2008) 127–137.
[33] H. Ziegler, in: I.N. Sneddon, R. Hill (Eds.), Progress in Solid Mechanics, vol. 4, John Wiley and Sons, New York, 1963, pp. 93–191.
[34] H.L. Gegel, J.C. Malas, S.M. Doraivelu, V.A. Shende, Metals Handbook, Forming and Forging, vol. 14, ASM International, Ohio, 1998, pp. 417–438.
[35] Y.V.R.K. Prasad, N. Ravichandran, Bull. Mater. Sci. 14 (1991) 1241–1248.
[36] R. Raj, Metall. Trans. A 12 (1981) 1089–1097.